FERNANDEZ-TOMAS, C. B. & BALTIMORE, D. (1973). *J. Virol.* **12**, 1122-1130.
FRENCH, T. J., MARSHALL, J. J. A. & ROY, P. (1990). *J. Virol.* **64**, 5695-5700.
FRIESEN, P. D., SCOTTI, P. D., LONGWORTH, J. & RUECKERT, R. R. (1980). *J. Virol.* **35**, 741-747.
GALLAGHER, T. M. (1987). PhD thesis, Univ. of Wisconsin, Madison, USA.
GALLAGHER, T. M. & RUECKERT, R. R. (1988). *J. Virol.* **62**, 3399-3406.
GUTTMAN, N. & BALTIMORE, D. (1977). *J. Virol.* **23**, 363-367.
HENDRICKSON, W. A. (1985). In *Methods in Enzymology*, Vol. 115, edited by H. W. WYCKOFF, C. H. W. HIRS & S. N. TIMASHEFF, pp. 252-270. New York: Academic Press.
HOEY, E. & MARTIN, S. (1974). *J. Gen. Virol.* **24**, 515-524.
HOSUR, M. V., SCHMIDT, T., TUCKER, R. C., JOHNSON, J. E., GALLAGHER, T. M., SELLING, B. H. & RUECKERT, R. R. (1987). *Proteins Struct. Funct. Genet.* **2**, 167-176.
KAESBERG, P., DASGUPTA, R., SGRO, J.-Y., WERY, J.-P., SELLING, B. H., HOSUR, M. V. & JOHNSON, J. E. (1990). *J. Mol. Biol.* **214**, 423-435.
KIM, S. (1989). *J. Appl. Cryst.* **22**, 53-60.
LUCKOW, V. A. & SUMMERS, M. D. (1988). *Biotechnology*, **6**, 47-55.
MCPHERSON, A. JR (1982). *Preparaion and Analysis of Protein Crystals.* New York: Wiley.
MATTHEWS, B. W. (1968). *J. Mol. Biol.* **33**, 491-497.
NEWMAN, J. F. E. & BROWN, F. (1973). *J. Gen. Virol.* **21**, 371-384.
NEWMAN, J. F. E. & BROWN, F. (1977). *J. Gen. Virol.* **38**, 83-95.
ROSSMANN, M. G. (1979). *J. Appl. Cryst.* **12**, 225-238.
ROSSMANN, M. G. & BLOW, D. M. (1962). *Acta Cryst.* **15**, 24-31.
ROSSMANN, M. G., LESLIE, A. G. W., ABDEL-MEGUID, S. S. & TSUKIHARA, T. (1979). *J. Appl. Cryst.* **12**, 570-581.
SCHNEEMANN, A. & RUECKERT, R. (1991). Personal communication, Univ. of Wisconsin, Madison, USA.
SCHNEIDER, I. (1972). *J. Embryol. Exp. Morphol.* **27**, 353-365.
SCOTTI, P. D., DEARING, S. C. & MOSSOP, D. W. (1983). *Arch. Virol.* **75**, 181-189.
TONG, L. & ROSSMANN, M. G. (1990). *Acta Cryst.* A**46**, 783-792.
URAKAWA, T., FERGUSON, M., MINOR, P. D., COOPER, J., SULLIVAN, M., ALMOND, J. W. & BISHOP, D. H. L. (1989). *J. Gen. Virol.* **70**, 1453-1463.

Acta Cryst. (1992). B**48**, 520–531

Structure Determination of a Dimeric Form of Erabutoxin-b, Crystallized from a Thiocyanate Solution

BY P. SALUDJIAN*† AND T. PRANGÉ‡

Chimie Structurale Bio-moléculaire (URA 1430 CNRS), UFR Biomédicale, 93012-Bobigny CEDEX, France

J. NAVAZA

Laboratoire de Physique, Faculté de Pharmacie, 92290-Chatenay-Malabry, France

R. MÉNEZ

Laboratoire d'Ingéniérie des Protéines, CEN Saclay, 91191-Gif sur Yvette CEDEX, France

AND J. P. GUILLOTEAU, M. RIÈS-KAUTT AND A. DUCRUIX

Institut de Chimie des Substances Naturelles, CNRS, 91198-Gif sur Yvette CEDEX, France

(*Received* 22 *September* 1991; *accepted* 21 *January* 1992)

Abstract

Erabutoxin-b, $M_r = 6861.1$, a single 62 amino-acid chain folded by four disulfide bridges, was crystallized in a new orthorhombic form by using thiocyanate as crystallizing agent. The space group is $P2_12_12_1$ with $a = 53.36$ (4), $b = 40.89$ (4), $c = 55.71$ (5) Å, $V = 121\,533.1$ Å^3 and $Z = 8$. X-ray diffraction data were recorded at the LURE synchrotron facility ($\lambda = 1.405$ Å). The structure was solved by molecular replacement and shows a dimeric association through an anti-parallel β-sheet around the twofold non-crystallographic axis. The two independent molecules, one SCN^- ion and 97 associated water molecules were refined by molecular dynamics and annealing techniques to $R = 19.6\%$ (10 913 F_{obs}, resolution 5–1.7 Å). The thiocyanate ion is located at the interface of the dimer and close to the non-crystallographic twofold axis.

Introduction

Crystal nucleation and growth are greatly affected by the type of salt used as the crystallizing agent. In a study of the influence of salts on solubility, it has

* Author to whom correspondence should be addressed.
† E-mail addresses: PS and TP at prange@frlure51; JN at ucba000@frors31; JPG, MRK and AD at ducruix@fricsn51
‡ Alternative address: LURE Bâtiment 209d, Université Paris-Sud, 91405-Orsay CEDEX, France.

0108-7681/92/040520-12$06.00

been demonstrated (Riès-Kautt & Ducruix, 1989, 1991) that, for basic proteins, thiocyanate ions can generate crystals at a much lower salt concentration than other ions. Taking advantage of this property, several proteins have been crystallized using thiocyanate ions including lysozyme (Riès-Kautt & Ducruix, 1989), fasciculine 1 (Ménez & Ducruix, 1990), muscarinic 2 (Ménez & Ducruix, 1991) and other snake toxins (unpublished data). In the case of erabutoxin-a and -b, a new crystal form was isolated.

Erabutoxin-b is a post-synaptic neurotoxin isolated from the venom of the sea-snake *Laticauda semifasciata*. It binds specifically to the nicotinic acetylcholine receptors with a high affinity ($K_d \cong 10^{-10}$ *M*, Dufton & Hider, 1983) and thereby blocks neuromuscular transmission. Erabutoxin-b belongs to the class of 'short' toxins. It comprises a single chain of 62 amino acids folded in β-sheets and loops, tightened by four disulfide bridges (see scheme below and Fig. 6), and displays the characteristic 'three-finger' structure, already encountered in several structurally related toxins (Drenth, Low, Richardson & Wright, 1980). [For a review on snake venom toxins, see Endo & Tamiya (1987) and Ménez (1987).] Its structure–function relationship has been reviewed by Low (1979).

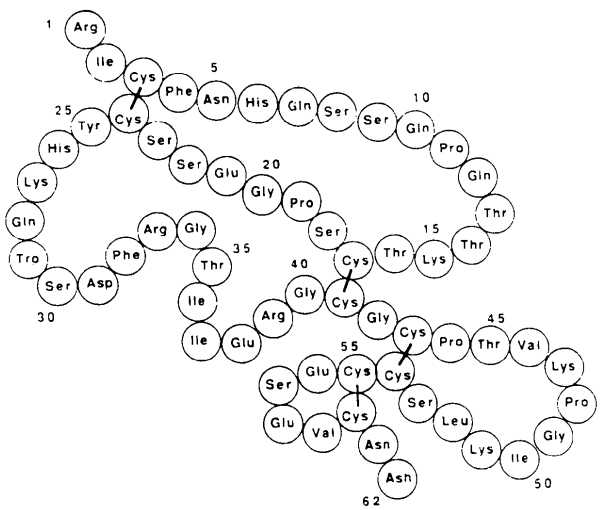

The three-dimensional structure of erabutoxin-b has been described previously (Low, Potter, Jackson, Tamiya & Sato, 1971; Low, Preston, Sato, Rosen, Searl, Rudko & Richardson, 1976). The structure of erabutoxin-b, crystallized from ammonium sulfate at pH = 7.5, was first refined at 2.2 Å (Tsernoglou & Petsko, 1976), then at 1.45 Å resolution (Low & Corfield, 1986; Smith, Corfield, Hendrickson & Low, 1988). The refined coordinates are available (codes 2EBX and 3EBX) in the Protein Data Bank (Bernstein, Koetzle, Williams, Meyer, Brice, Rodgers, Kennard, Shimanouchi & Tasumi, 1977).

In order to determine whether the SCN^- ion could be located within the crystal the X-ray determination of this new crystal form was undertaken.

Material and methods

Crystallization

Lyophilized erabutoxin-b was kindly supplied to us by Dr A. Menez (Service de Biochimie des Protéines, CEN Saclay). The crystallization experiments were performed using the vapor-diffusion technique. Hanging drops of 10 µl, containing the protein (3 m*M*), KSCN (0.15–0.2 *M*) as crystallizing agent, and acetate buffer (50 m*M*, pH = 4.5) were equilibrated against a 0.3–0.4 *M* KSCN reservoir maintained at the same pH. Crystals normally appear within two weeks. The largest crystals grow to more than 1 mm in length with a 0.3×0.3 mm^2 square cross section.

Data collection and processing

The diffraction data were collected on film using the rotation method. Crystal rotations of $\Delta\omega = 3°$, without overlap between successive exposures, were performed at a wavelength of $\lambda = 1.405$ Å, selected by a curved Ge(111) monochromator, at the D43 synchrotron beam port at LURE, Orsay. The crystal-to-film distance was fixed at 4.9 cm, corresponding to a maximum resolution of 1.7 Å ($2\theta \leq 48.8°$ and *hkl* range 0–31, 0–24, 0–32) at film edges. Three films were used per pack and all data were collected on a single crystal ($1.6 \times 0.3 \times 0.3$ mm). The *c* axis, which corresponds to the length of the crystal, was aligned along the camera rotation axis. Taking advantage of the nearly parallel X-ray beam and using a 0.2 mm collimator, a spindle translation was made every 30° of accumulated data in order to expose a different portion of the crystal. This led to a reasonable crystal lifetime (roughly two days). The overall ω range covered was 92°; portions of the blind region were also recorded from a second crystal but this data set was found to be of poor quality after the complete treatment of intensities and was therefore not included in either the structure determination or subsequent refinement.

The films were scanned using an Optronics P1000 photoscan densitometer with a 50 µm raster step. The corresponding core images were processed up to 1.7 Å resolution using the *DENZO* program (Otwinowski, 1988). The indexed intensities were converted into the LCF format (*CCP*4, 1979) through a local program. This resulted in a total of 33304 observations. After scaling and merging intensities using the Fox & Holmes (1966) algorithm *ROTAVATA/AGROVATA*, which takes into account crystal degradation and beam intensity

variations (programs from *CCP*4, 1979), 11227 independent fully recorded reflections were obtained with an overall merging R factor ($\sum|I - \langle I\rangle|/\sum I$) on intensities of 4.9%. Standard corrections were applied for both Lorentz and polarization factors but no absorption corrections were made. Because post-refinement was not applied, the partial reflections were not included. The intensities were converted to structure-factor amplitudes (*TRUNCATE*, French & Wilson, 1978). The final completeness was 82% up to 1.70 Å (64% in the range 1.82–1.70 Å, comprising 1577 F_{obs}).

The crystals obtained in the presence of KSCN are orthorhombic with unit-cell parameters $a = 53.36$ (4), $b = 40.89$ (4), $c = 55.71$ (5) Å. Because of systematic absences for only the $h00$, $0k0$, $00l$ zones, the space group was uniquely determined as $P2_12_12_1$ with four equivalent positions. These parameters and space group were also confirmed on a Philips PW1100 four-circle automatic diffractometer, from the angular settings of 25 randomly distributed reflections followed by least-squares refinement of the corresponding UB matrix (Busing & Levy, 1967).

The experimental density D_m was not measured. The calculated value for the partial specific volume of erabutoxin-b is 0.71 $cm^3\ g^{-1}$ (Tamiya & Arai, 1966). A single molecule of erabutoxin-b, molecular weight 6861, having such a partial specific volume would occupy approximately 27% of the volume of the asymmetric unit leaving 73% for the liquid of crystallization.

Table 1 reports the erabutoxin-b crystal parameters from both ammonium sulfate (Low *et al.*, 1971) and thiocyanate crystallization conditions. It becomes evident, from the hydrated molecular volumes V/n, that two molecules are present in the asymmetric unit thus giving a hydration content of 47%. In this particular case, molecular replacement was the method of choice for determining the location of the molecules in this new cell habit.

Table 1. *Crystal parameters for erabutoxin-b*

	2EBX/3EBX*	Present
Source	$(NH_4)_2SO_4$	KSCN
a (Å)	49.94	53.36
b (Å)	46.58	40.89
c (Å)	21.59	55.71
V (Å^3)	50223	121553
Space group	$P2_12_12_1$	$P2_12_12_1$
$V/4$ (Å^3)	12555	30388
$V/8$ (Å^3)	6278	15194
Z	4	4
Hydration (%)	34	47

* Codes are from the PDB (Bernstein *et al.*, 1977).

Structure determination

The strategy adopted was a combination of the following steps: determination of the orientation of the molecules by a *rotation function*, determination of the positions of the oriented molecules by a *translation function* and *rigid-body refinement*.

(1) The rotation functions in different versions of three different packages were investigated: the *ALMN* and *POLARRFN* functions from the *CCP*4 suite of programs (1990 version), the *MERLOT* package (Fitzgerald, 1988) and the *ROTING* program described by Navaza (Navaza, 1987, 1990).

(2) Upon rotation of the model molecule (by the angles derived from the rotation-function analysis), a three-dimensional Crowther–Blow (Crowther & Blow, 1967) translation search was systematically made for each angular triplet corresponding to the ten highest rotation peaks. The *TFSGEN* program included in the *CCP*4 package, based on Tickle's formulation (Tickle, 1985), was employed with a grid step of approximately 0.5 Å (108 points along **a** and **c**; 84 along **b**). In the particular case of the space group $P2_12_12_1$, each of the independent molecule translation parameters is defined as modulo $\frac{1}{2}$, on the three axes. When two sets of parameters are considered together – the two independent molecules of the asymmetric unit – the eight possible arrangements of the second molecule with respect to the first (origin fixing), have to be explored.

(3) The best rotation/translation parameters were systematically refined by three different methods: *MERLOT*'s *RMIN* function, the rigid-body refinement option of the *XPLOR* program (Brünger, 1990), and a fast group-refinement procedure (Huber & Schneider, 1985), implemented in the *FITING* program (Castellano, Oliva & Navaza, 1992).

Cross-rotation

All atoms of the 2EBX erabutoxin-b structure, initially translated with the origin at the barycentre, were used as the search model. This model was placed in a P_1 orthogonal unit cell of 65 Å edge. It was chosen by adding the maximum dimensions of the molecule (35 Å), the maximum radius of integration tested (25 Å) and a boundary of 5 Å. The cross-rotation maps were calculated using the 10 to 3 Å data and a Patterson cut-off radius (r_{Patt}) in the range 15 to 25 Å. The search grid was $\Delta\alpha = 2.5$, $\Delta\beta = 5$ and $\Delta\gamma = 2.5°$. In our case the *mmm* symmetry leads to a set of four equivalent positions at α, β, γ; $\pi + \alpha$, β, γ; $\pi - \alpha$, $\pi - \beta$, $\pi + \gamma$; $2\pi - \alpha$, $\pi - \beta$, $\pi + \gamma$ (Moss, 1985).

Several runs of *MERLOT* were tried using slightly different modifications of the parameters quoted above: in all cases, only one strong peak was found to emerge constantly from the Euler angle maps (Table 2).

The *ROTING* program, which is a modification of the Crowther formulation (Crowther, 1972), gave the

Table 2. *Results of the fast-rotation function (MERLOT) using the 2EBX structure as model*

Data used to calculate harmonic coefficients were from 10 to 3.8 Å with a radius of integration of 16 Å.

Peak rank	α (°)	β (°)	γ (°)	Peak height R.m.s.	Peak height % max.
1	137.5	65	115	3.6	100
2	157.5	105	230	3.2	88
3	127.5	85	145	3.1	85
4	157.5	102	230	3.0	84
5	172.5	67	115	2.9	82
6	120.0	37.5	185	2.8	79
7	165.0	102	255	2.8	78
8	162.5	62.5	95	2.7	74
9	112.5	70	185	2.6	71
10	170.0	120	250	2.5	67

Table 3. *Results of the fast-rotation function (ROTING) using the 2EBX structure as probe, including all L coefficients*

Data used to calculate harmonic coefficients were from 10 to 3 Å with a radius of integration of 15 Å. The correct solution is ranked first.

Peak rank	α (°)	β (°)	γ (°)	Peak-height correlation	Highest peak ρ = height/r.m.s. (in translation)
1	139.4	64.7	116.6	20.3	10.1
2	129.0	86.0	141.5	17.7	5.1
3	147.2	76.5	141.5	17.7	4.9
4	52.4	90.0	324.6	16.4	5.2
5	156.7	68.0	125.0	16.0	5.0
6	162.9	80.2	153.7	15.4	4.8
7	176.6	76.3	145.6	15.2	4.9
8	123.3	38.5	180.1	15.2	4.1
9	108.5	86.8	178.9	14.8	5.3
10	15.0	83.3	153.6	14.5	5.1

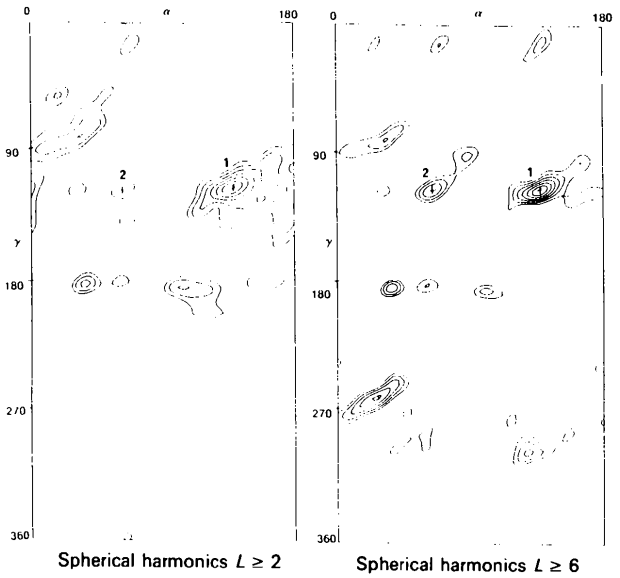

Fig. 1. *ROTING* cross-rotation functions (section: $\beta = 65°$) calculated with the same optimized parameters used in *MERLOT*. The omission of $L < 6$ (right) sharpens and increases the height of the peak corresponding to the second solution (+2).

best results. The direct output of this program (Table 3) is the correlation coefficient. Fig. 1 (left) displays the best contrasted map obtained with $r_{Patt} = 21$ Å and a resolution range from 8 to 3.5 Å. This solution is close to one obtained with *MERLOT* when employing the same set of input parameters.

Translation

For each of the ten highest peaks emerging from a rotation map, a translation function was automatically calculated. This usually gave, in most cases, one or two translation solutions with a ratio ρ = (peak height)/r.m.s. of the order of 5. However, the top rotation peak was the only one to give a single well-defined translation solution with a ratio of $\rho \cong 10$. Based on this criterion, no solution was revealed for the second orientation in the ten top peaks (Tables 2 and 3).

Rigid-body refinement

To assess the correctness of the individual molecular positions, systematic rigid-body refinements were carried out using the *RMIN* program in the *MERLOT* package and the *FITING* program, as described above.

For the ten top solutions of the rotation/translation procedure, the *R* factors ranged from 59 to 69% with *RMIN*, and from 53 to 60% with *FITING*. Even if the first solution gave the smallest *R* value, the others were close, indicating that the conventional *R* factor is not discriminative. However, the correlation factor obtained from *FITING*, (25% for the first orientation and between 5 and 13% for the others) is a better figure of merit and confirms the results of the translation function. At this stage, only one solution gave both a good ρ ratio and a good correlation factor.

A packing test was performed to verify the model consisting of two molecules in the asymmetric unit. Each model consisted of the first top solution plus one of the remaining nine peaks, origin-translated in one of the eight possibilities described above. The *XPLOR* program was used, as indicated previously, jointly with *FITING*. In all cases, a preliminary packing analysis pointed to some partial overlap between the two molecules.

All of these models gave *R* factors in the range 60–55% and correlation coefficients in *FITING* less than 22%. It was thus clear that the position of the second molecule remained undetermined at this stage.

Self-rotation

The self-rotation of the Patterson function was run in parallel. The *POLARRFN* function was calculated

using 10 to 3 Å data, with inner and outer Patterson cut-off radii of 3 and 15 Å. A set of strong maxima, representing 45% of the normalized peaks for the crystallographic axes, was observed at $\omega = 90$, $\varphi = 35$ and $\kappa = 180°$ (in polar coordinates, Fig. 2). This corresponds to a set of twofold non-crystallographic symmetry axes relating the two independent molecules in the unit cell.

Similar results were obtained with the program *ROTING*, but not with *ALMN* and *MERLOT*. It is interesting to note that, with the exception of the crystallographic axes, these self-rotation peaks were the unique isolated maxima in the whole map.

After applying this twofold rotation to the best solution of the cross function, the resulting new set of orientation angles gave, in the translation test, a ρ ratio of 11 together with a correlation factor of 20% and a satisfactory packing analysis. The *XPLOR* and *FITING* results for the eight possible positions of the second molecule with respect to the first (fixed) are given in Table 4: the results of *XPLOR* clearly indicated set 4 to be correct, with a conventional R value of 47% (including 1928 F_{obs} at 3.2 Å resolution). The contrast is even more striking when using the correlation coefficient given by *FITING*.

A posteriori methodological analysis

The solution was thus found in several steps, each one needing an independent analysis. Normally, the cross-rotation (first step) would have given the orientations of both independent molecules in the asymmetric unit. The inability to reveal a second reliable orientation was solved with the help of the self-rotation solution, which was extremely clear in our case. This situation is not satisfactory from a methodological point of view and should stimulate further improvements of cross-rotation functions.

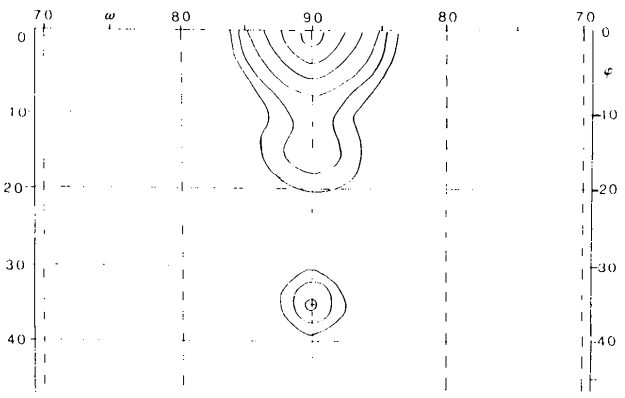

Fig. 2. Part of the orthogonal projection of the self-rotation function in polar coordinates (section $K = 180°$). The single maximum at ($\omega = 90$, $\varphi = 35°$) is 45% of the 2_1 crystallographic axis ($\omega = 90$, $\varphi = 0°$).

Table 4. *Rigid-body refinements of peak* 1 *plus origin-translated peak* 2

The correct solution is set 4. Selected values: peak 1 ($\alpha = 137.5$, $\beta = 65.0$, $\gamma = 115.0°$, $T_x = 0.1944$, $T_y = 0.2381$, $T_z = 0.4074$); peak 2 ($\alpha = 115.2$, $\beta = 116.0$, $\gamma = 294.5°$, $T_x = 0.1018$, $T_y = 0.1429$, $T_z = 0.4444$).

Set	Peak 1 + (Peak 2 + translations)			*XPLOR* R (%)	*FITING* R (%)	*FITING* Correlation coefficient
1	0	0	0	67	52.9	24.9
2	$\frac{1}{2}$	0	0	65	52.8	25.2
3	0	$\frac{1}{2}$	0	64	51.5	27.2
4	0	0	$\frac{1}{2}$	47	43.4	50.7
5	0	$\frac{1}{2}$	$\frac{1}{2}$	66	52.9	24.8
6	$\frac{1}{2}$	0	$\frac{1}{2}$	64	51.4	27.2
7	$\frac{1}{2}$	$\frac{1}{2}$	0	63	51.5	26.6
8	$\frac{1}{2}$	$\frac{1}{2}$	$\frac{1}{2}$	67	53.2	23.3

A closer examination of the cross-rotation map shows *a posteriori* that in general, the second solution is present among the hundred top peaks. In our case, *ROTING* gave this second orientation in the 36th position. However, one of the additional features of this program is that it allows the removal of low-order terms of the harmonic coefficients, which enhances the angular resolution of the map (Navaza, 1987). In the present case the first peak remained unchanged, but not the following ones (Table 5 and Fig. 1, right). The second correct orientation now appears at rank seven.

The first step of *ROTING* is rather fast in terms of c.p.u. time. For example, the cross-rotation function using data to 3 Å and a cut-off radius of 15 Å (which involves 26 l terms plus 2323 and 16 069 reflections for the crystal and the model respectively) takes about half an hour on a MicroVAX II.

The translation function (second step) is also rather fast (3 min of c.p.u. time 1316 reflections up to 3.6 Å), although it involves a preliminary calculation of Fourier coefficients for each given orientation of the model molecule.

The third step (program *FITING*) allows for a quick and reliable evaluation of the quality of possible solutions generated by the preceding steps (Table 6). For example, under the same conditions as in step two, it takes 10 s of c.p.u. time per iteration.

This suggests that, providing a number of the *ROTING* solutions are explored, an automated procedure* may be set up to solve the crystal structures by molecular replacement. This was almost done in the present case, but due to the manual interfaces between the programs in the three steps described, a limited number of orientations and positions were tested. The number of orientations to be analyzed may be reduced further, if one only keeps the common peaks given by *ROTING*, obtained

* A package is currently under development (J. Navaza & M. Sarrazin, to be published).

Table 5. *Results of the fast-rotation function (ROTING) using the 2EBX structure as probe, removing L = 2, 4*

Data used to calculate harmonic coefficients were from 10 to 3 Å with a radius of integration of 15 Å. The solutions are ranked first and seventh.

Peak rank	α (°)	β (°)	γ (°)	Peak-height correlation
1	137.8	65.5	114.7	16.7
2	153.4	39.9	77.3	14.2
3	26.6	64.2	260.5	13.7
4	106.1	23.1	169.3	13.2
5	40.2	33.1	172.7	13.0
6	74.3	56.7	96.4	12.9
7	63.4	67.3	116.1	12.6
8	122.6	38.5	178.7	12.4
9	55.6	83.5	141.8	12.2
10	36.7	62.0	182.6	11.9

Table 6. *Results of the translation and rigid-body refinement with FITING for the orientations given in Table 5*

Data used from 10 to 3.6 Å, solutions are ranked first and seventh.

Peak rank	Starting translations T_x	T_y	T_z	ρ	Correlation	R (%)
1	0.1944	0.2381	0.4074	11.1	21.3	54.3
2	0.1111	0.2619	0.0000	4.2	9.2	57.8
3	0.4074	0.3929	0.1111	4.4	2.5	60.1
4	0.2870	0.2619	0.4630	4.6	10.7	58.1
5	0.3241	0.4762	0.0463	4.5	4.9	58.3
6	0.1759	0.1548	0.3148	4.4	9.4	58.1
7	0.3981	0.1429	0.0556	6.6	18.2	55.8
8	0.1481	0.4881	0.3704	4.7	7.6	58.3
9	0.4352	0.3214	0.2685	4.4	8.0	57.8
10	0.3519	0.3929	0.2685	4.7	6.5	57.8

from different starting L's (this involves no extra computing time, since the expansion coefficients in spherical harmonics are only calculated once). Furthermore, the above three steps need a single calculation of the Fourier coefficients corresponding to the model molecule.

Structure refinements

The two independent molecules of the structure were refined using the *XPLOR* molecular dynamics program (Brünger, 1990). The starting point for refinement was the structure of the monomeric form of erabutoxin-b 2EBX (Protein Data Bank, Bernstein *et al.*, 1977) oriented and translated according to the molecular replacement solutions and after the rigid-body refinement described in Table 4. None of the non-crystallographic symmetry information (NCS) was applied during the refinement (see Table 7). Parameters were adjusted so as to include the protonated state for basic amino acids. After several cycles of crystallographic/dynamic refinement, with a step-by-step increasing resolution from 3.2 to the maximum resolution of

Table 7. *Refinement parameters and progress of the R factor as a function of refinement steps*

1 kcal = 4.1868 kJ.

Step	Description	E_{total} (kcal)	E_{rx} (kcal)	R (%)/ resolution (Å)
1	Determination of weights $Wa = 45000$; $wp = 1$	2×10^4	1.2×10^3	38.3/2.2
2	80 cycles of conjugate gradient refinement (X-ray and energy minimization) in six steps from 3.2 to 1.7 Å	138	7×10^2	29.0/1.7
3	Temperature cooling from 2200 to 290 K, total time = 3 ps, by steps of 1 fs	0.2	11	25.1/1.7
4	Graphics inspections, water localizations	1×10^3	98	22.0/1.7
5	40 cycles of conjugate gradient refinement; loops step 4			
6	Final values	−2.8	+1.8	19.6/1.7

1.7 Å, a slow-cooling annealing procedure was applied (from 2200 to 290 K). The R value was lowered to 25% (9095 F_{obs}; 1.75 Å resolution). Graphic inspection of $2|F_o| - |F_c|$ and $|F_o| - |F_c|$ maps using *FRODO* (Jones, 1978) revealed a large number of water molecules, with correct bond distances and angles and pointing towards the backbone polar atoms. These were included in the atomic model contribution with an initial isotropic B factor equal to 25 Å^2. The highest peak observed in the $|F_o| - |F_c|$ map was an elongated 'bottle-like' electron density region located at the interface of the two molecules of the asymmetric unit. This density was immediately attributed to a thiocyanate ion (Fig. 3). The refined protein model required only minor manual adjustments:

(i) The His26 side-chain ring had to be flipped upside down in both independent molecules, to fit the correct hydration scheme (Fig. 4).

(ii) The Phe32*B* side chain lay outside the electron density and had a twisted geometry – probably due to disorder.

The crystallographic/dynamic refinement was continued with 70 molecules of water (full occupancy parameters) and one thiocyanate ion. The thermal factors of the water molecules were used as a probe and were not allowed to exceed a threshold value of 60 Å^2. If this occurred they were discarded and new relocation steps were restarted on difference maps in order to obtain more peaks. This procedure proved to be very sensitive for the first hydration shell, no attempts were made to take residual densities into account by giving partial occupancies to additional water molecules; *i.e.* those directly connected to the protein. Only eight water molecules belonging to the second hydration sphere were refined with variable occupancy factors and a fixed B factor equal to the average value of all water molecules in the first shell (28.5 Å^2). The final R-value analysis is detailed in Table 8 (resolution 1.7 Å, R = 19.6% using 10 913

$F_{obs} > 2\sigma$; and $R = 17.7\%$, 6785 $F_{obs} > 4\sigma$). The final model includes two molecules of erabutoxin-b, 97 water molecules (89 in the first hydration shell; eight in the second) and a thiocyanate ion.

Fig. 5 depicts a portion of the $|F_o| - |F_c|$ density contouring (5σ level, 1.7 Å resolution) of the Tyr25 side chain and clearly shows the quality of the map.

A the end of the *XPLOR* refinement step 4 (Table 7), the ring planarities of some aromatic side chains (His6, Phe32 and Trp29) were found to be somewhat distorted, even using very high energy terms for the improper definitions. This was also the case for a few peptidic linkages. The inclusion of water molecules in the model immediately brought back the overall geometry to a better agreement, a behaviour which emphasizes the fact that water molecules must be included as early as possible in the high-resolution refinement steps. This feature was previously reported in the case of an octanucleotide structure at 1.7 Å (Kennard, Cruse, Nachman, Prangé, Shakked & Rabinovitch, 1986). Finally, the ring planarities were completely restored without increasing the R factor by applying ten cycles of *PROLSQ* refinement (Konnert & Hendrickson, 1980; Hendrickson, 1985).

Table 9 shows the final statistics of the model geometry after the last cycle of refinement.* The r.m.s. coordinate shifts in the last cycle were $\cong 0.002$ Å, and the overall r.m.s. deviations are 0.025 Å and 2.1° on distances and angles, respectively.

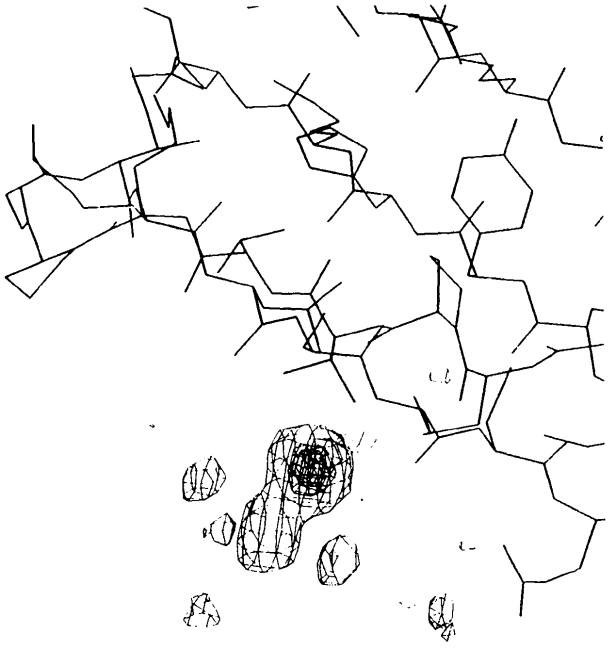

Fig. 3. $|F_o| - |F_c|$ map showing the thiocyanate ion at the surface of molecule *A* (resolution 1.7 Å) at the two 2σ and 5σ contouring levels.

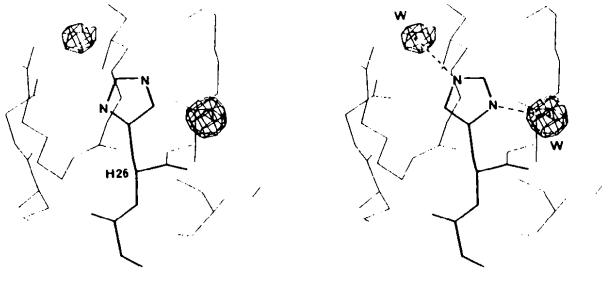

Fig. 4. $|F_o| - |F_c|$ map calculated before location of the water molecules (step 4 in Table 7): Aspect of the His26 side chain and surrounding water molecules (left). There is a clear indication that this residue has to be rotated 180° to fit the hydration scheme correctly (right). The use of the *B* thermal-factor distribution (Waller & Liddington, 1990) was not relevant in our case.

Table 8. *Analysis of the R factor versus the resolution and versus the intensities of the structure factors for the last refinement cycle*

Resolution (Å)	No. F_{obs}	R(shell)	R(cum.)	Amplitudes	No. F_{obs}	R(shell)	R(cum.)
20.0–3.40	1571	0.211	0.211	72–204	5085	0.293	0.293
3.40–2.70	1557	0.196	0.201	204–335	3048	0.198	0.210
2.70–2.36	1484	0.183	0.192	335–466	1163	0.174	0.204
2.36–2.14	1436	0.181	0.186	466–597	503	0.161	0.200
2.14–1.99	1362	0.189	0.187	597–728	256	0.139	0.199
1.99–1.87	1193	0.198	0.190	728–860	109	0.137	0.198
1.87–1.78	1060	0.215	0.194	860–990	55	0.127	0.196
1.78–1.70	571	0.228	0.196	990–1120	15	0.085	0.196

Discussion

Erabutoxin-b is folded into three adjacent loops rich in β-pleated sheets which protrude from a small globular core made rigid by four disulfide bridges (Fig. 6).

This folding is commonly observed in neurotoxins and cardiotoxins. It displays the characteristic 'three-finger' structure with a concave bowl-shaped face. The orientation of this concavity characterizes the cardiotoxin group from the post-synaptic neurotoxin group. In the neurotoxin group itself, important homology can be observed (Low, 1979). The five residues Phe32, Ile36, Glu38, Ile50 and Leu52 (Fig. 6) are some of the common invariant residues in all short and long toxins and they are considered to be responsible for the high affinity ($K_d \cong 10^{-10}$ *M*) towards the receptor.

* Atomic coordinates and structure factors have been deposited with the Protein Data Bank, Brookhaven National Laboratory (Reference: 6EBX, R6EBXSF), and are available in machine-readable form from the Protein Data Bank at Brookhaven. The data have also been deposited with the British Library Document Supply Centre as Supplementary Publication No. SUP 37062 (as microfiche). Free copies may be obtained through The Technical Editor, International Union of Crystallography, 5 Abbey Square, Chester CH1 2HU, England.

Fig. 7 shows plots of temperature factors averaged over amino-acid atoms for the two independent molecules together with the original monomeric refined structure (2EBX). The cysteine residues are indicated by vertical arrows. The hinge points determined by the disulfide bridges usually correspond to residues with the lowest B values, the loop regions to the highest (this corresponds to regions 6→9, 30→34 and 44→52). The diagram emphasizes the good alignment of the thermal factors with those of the original monomeric form, including the 'hot region'* formed by the third finger loop (44→52). In 3EBX (Smith *et al.*, 1988), this region was constructed as two 60:40 weighted disordered chains, but as a single chain in the previously refined 2EBX (Low & Corfield, 1986). As far as the present structure is concerned *i.e.* with two molecules A and B in the asymmetric unit, the $30B$→$34B$ region (the second finger loop) also exhibits unusually high averaged thermal factors. No alternative chain tracing in the region $30B$→$34B$ was observed when using omit maps. However a graphic inspection showed some degree of disorder in the Phe32B side chain but not in the main chain itself. This was treated as two different weighted (65:35) orientations. The corresponding region in molecule A is not disordered.

The average B factors in both independent molecules, are $\langle B\rangle_A = 10.4$ and $\langle B\rangle_B = 14.6$ Å^2, for the main chains, and $\langle B\rangle_A = 14.7$ and $\langle B\rangle_B = 18.8$ Å^2, for the side chains. This indicates a slightly high degree of motion/disorder in molecule B with respect to A. Fig. 7 shows that the curve corresponding to B is above the alignment of molecule A and above the values of the monomeric 2EBX structure. However this is only true for residues 1 to 40, which correspond to fingers 1 and 2. A packing effect due to the association can be observed as this situation is reversed for the third finger, around which the two molecules are linked by intermolecular β-sheet: the 2EBX monomeric average $\langle B\rangle$ curve is now above the other two.

A φ/ψ plot (Ramakrishnan & Ramachandran, 1965) is shown in Fig. 8. It is typical of pure β-sheet structures, with the exception of the glycine residues (circles in Fig. 8), where the torsion angles are influenced by the lack of a side chain. In this diagram, two residues deviate from the minimum energy region: Ser8 and Arg33 in molecules A and B. This structural high-energy bend is also observed in the 2EBX structure refined previously (Low & Corfield,

* This description is valid from both a biochemical point of view, *i.e.* interactions at the receptor, and from a crystallographic point of view, as a highly agitated region.

Table 9. *Final r.m.s. standard deviations after the last cycle of refinement*

Some definitions are from a last calculation with *PROLSQ* [ΔF modeled as 25–250(1–0.1888s), $s = \sin\theta/\lambda$].

	No.	Target σ	Actual σ	No. deviating $>2\sigma$
Distances (Å)				
Atoms 1–2 distances	980	0.015	0.019	10
Angles 1–3 distances	1325	0.025	0.029	33
Planar 1–4 distances	326	0.040	0.048	7
Planar groups	166	0.015	0.019	4
Chiral volumes (Å^3)	138	0.080	0.130	11
Torsion angles (°)				
Peptide planes	128	2.00	3.10	12
Staggered	174	15.0	15.0	8
Orthonormal	12	18.0	17.0	0

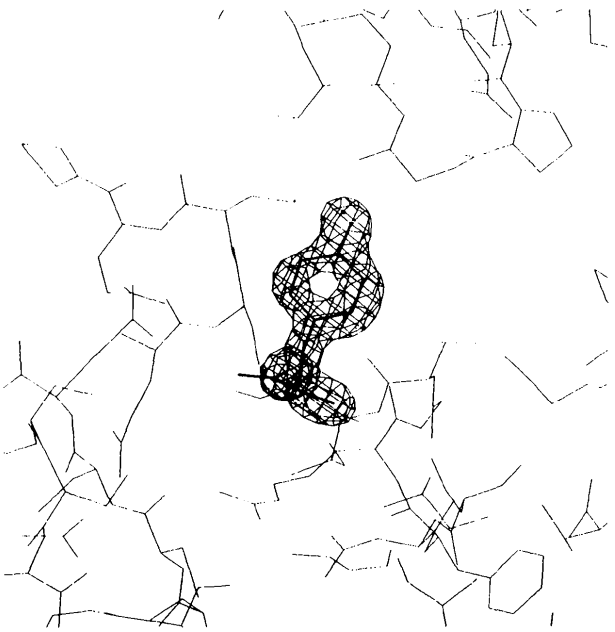

Fig. 5. Part of a final difference map for the Tyr25 residue at 1.7 Å resolution, calculated at the end of the refinement (5σ level).

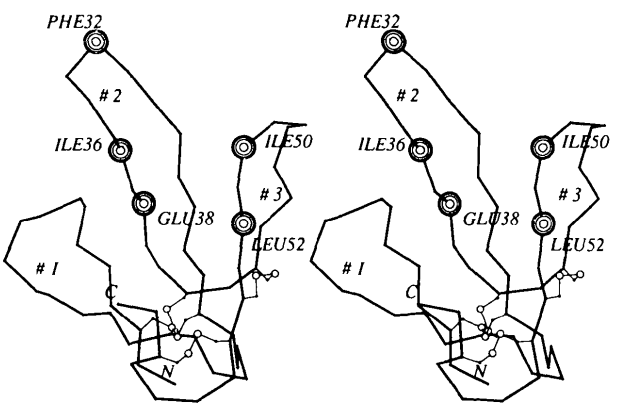

Fig. 6. The C_α backbone of the monomer A of erabutoxin-b with the four disulfide bridges (small open circles) located at the bottom of the structure. The three 'fingers' are labelled, and the conserved residues in fingers 2 and 3 are shown as filled circles.

1986). Both are located in β-turns at the ends of the first and second fingers. As mentioned above, they are also implicated in a region of high thermal factors. The corresponding residue in the third finger is also a glycine.

Comparisons of the different conformations in the dimer

Fig. 9 illustrates the least-squares minimization of the two C_α tracings of the subunits together, as well as a least-squares fit of molecule *A* over the 2EBX structure (Bourne, Sato, Corfield, Rosen, Birken & Low, 1985). In the two independent molecules of erabutoxin-b/KSCN the main-chain conformations are very similar, with r.m.s. deviations in the range 0.4–0.5 Å, including the 'hot' loop at the end of finger 2 which differs significantly in local conformation. All of these r.m.s. values, as well as those calculated when comparing both *A* and *B* molecules with the original erabutoxin/$(NH_4)_2SO_4$ structure, are reported in Table 10. The immediate feature which stands out is the close conformational identity of erabutoxin-b C_α main chains in all cases, though not for the side chains which adopt rather different orientations. In other words, this new packing arrangement has little effect on the overall C_α backbone conformation of the erabutoxin-b molecules but significantly affects the side-chain orientations after the third atom (C_γ *etc.*), when they are present.

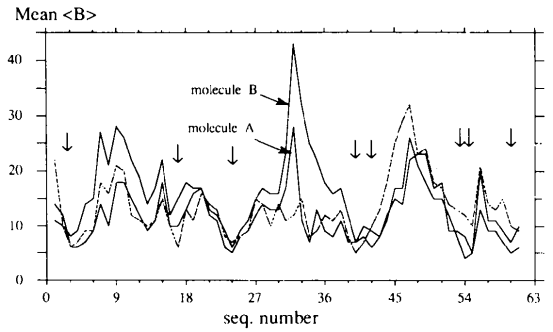

Fig. 7. Thermal analysis of the *B* factors *versus* the sequence for molecules *A* and *B*, compared to the original (2EBX) structure (dotted lines). Averaged $\langle B \rangle$ values (Å^2) are: 10.4/14.6 for *A*/*B* main chains (226 atoms); 14.7/18.8 for *A*/*B* side chains (249 atoms); 28.5 for waters (97 molecules) and 25.8 for the SCN^- ion (3 atoms).

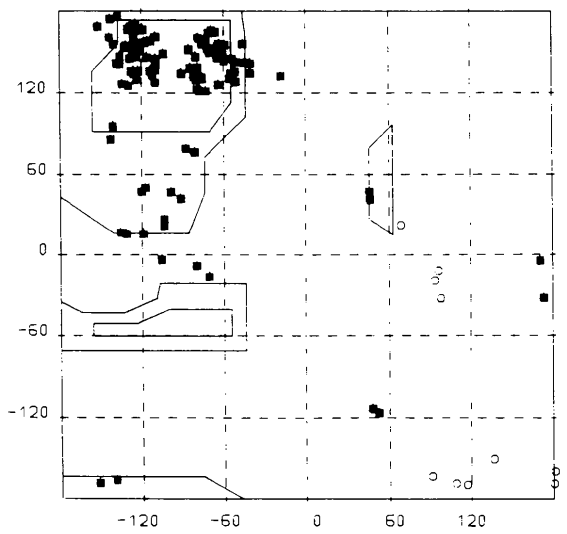

Fig. 8. Ramachandran plot of the peptide angular distribution for the φ/ψ parameters in the two molecules *A* and *B*. (Glycine residues are indicated by circles.)

Packing interactions between the two subunits

It is interesting to note that association of the two independent molecules does not just build a dimeric structure, as observed in many enzymes or proteins, followed by the packing of discrete dimers, but it is the result of a more general interacting network distributed all over the crystal packing. These features can be classified as follows: (1) an intermolecular anti-parallel β-sheet association between finger 3 of *A*[1 000] and molecule *B*[1 000] (Figs. 10

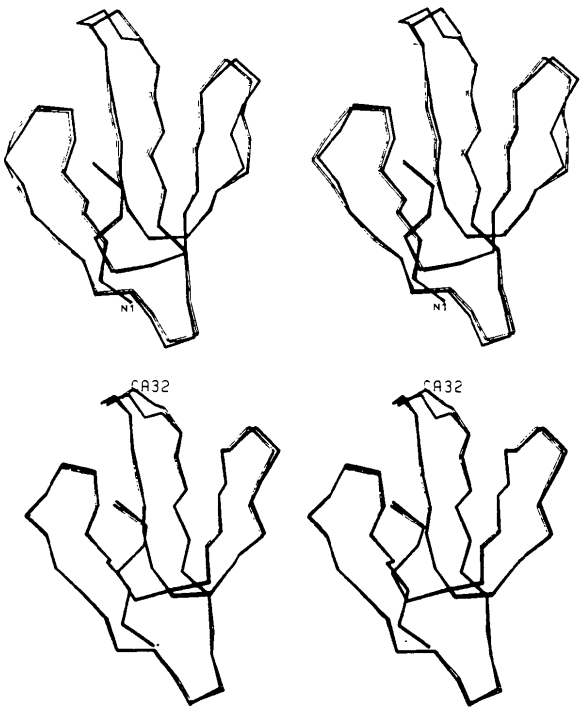

Fig. 9. (Upper) Stereoscopic pairs of the least-squares best molecular fit of the C_α backbones in the two independent molecules. Average r.m.s. values are given Table 10. Bold and light lines for molecules *A* and *B*, respectively. (Lower) Least-squares fit of molecule *A* (bold line) and the monomeric 2EBX structure.

Table 10. *Average r.m.s. values* (Å) *for least-squares minimizations*

Type of atoms used	No.	*A*/*B*	2EBX/*A*	2EBX/*B*
Main-chain atoms: C, N, C_α	186	0.41	0.78	0.75
or C_α—C_β—C—N—O atoms	342	0.52	0.90	0.86
C_γ—N and O atoms in side chains	133	1.79	2.04	1.63
C_α loop finger 1 (7→11)	20	0.33	1.01	1.00
C_α loop finger 2 (30→33)	16	1.24	1.66	1.37
C_α loop finger 3 (47→50)	16	0.69	1.26	0.96

and 12);* (2) a head-to-head interleaving of fingers 2 and 3 between *A*[1 000] and *B*[2 000] with a double interaction of Phe32*A*/Trp29*B* and Trp29*A*/Phe32*B* aromatic side chains (Fig. 11); (3) an interaction *via* the thiocyanate ion located close to the intermolecular β-sheet, in a pocket delimited by three molecules of the packing (one *B* and two *A*, Fig. 13); (4) cross-linking water molecules with side chains of polar residues located at the interface.

(1) *The anti-parallel β-sheet association.* This association in the dimer implies four H bonds (N↔O short distances) in the range 2.8–3.1 Å (Table 11) between the same amino acids, 52 to 56 in both molecules, around the non-crystallographic twofold axis (Fig. 10). One notices that the dimeric arrangement *via* intermolecular β-sheet association through the same side of finger 3 is the usual mode of auto-association observed in several snake venom toxin crystal structures, including α-bungarotoxin (Love & Stroud, 1986) and cardiotoxin (Rees, Samama, Thierry, Gilibert, Fischer, Schweitz, Lazdunski & Moras, 1987; Rees, Bilwes, Samama & Moras, 1990). The resulting regular and continuous six strand β-sheet twist thus obtained is characteristic of the group despite significant differences observed between erabutoxin-b and the two cardiotoxin and α-bungarotoxin X-ray structures.

(2) *The head-to-head interaction.* Fig. 11 shows how the two molecules *A*[1 000] and *B*[2 000] interact in the packing *via* the interleaving of fingers 2 and 3. This is achieved through a number of short polar contacts where Ser30*B* plays a key role as described

* Symmetry codes are given in square brackets as usual: the first number is the symmetry operation [as given in *International Tables for Crystallography* (1983, Vol. A)], followed by the translation units along the three axes to the molecule at closest approach. Letters *A* and *B* refer to the two independent molecules, respectively.

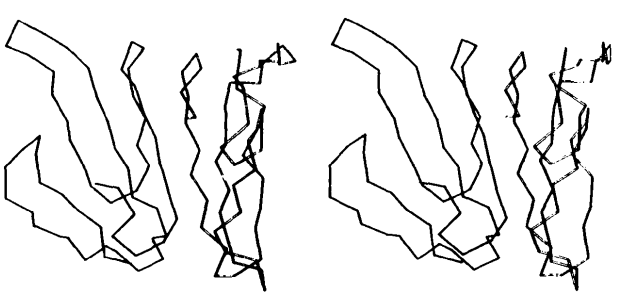

Fig. 10. The β-sheet association of the two independent molecules *A*[1 000] and *B*[1 000]. The O→N distances in the intermolecular anti-parallel β-sheet are reported Table 11.

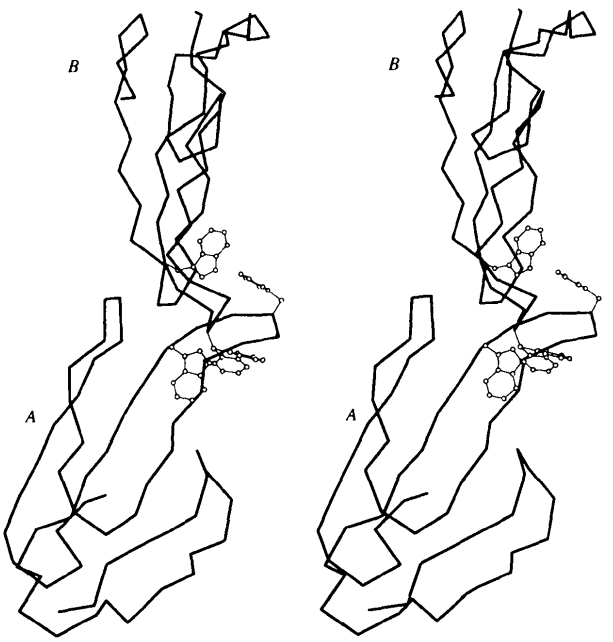

Fig. 11. The head-to-head interleaving interactions of fingers 2 and 3 displaying the *F*/*W* interactions between *A*[1 000] and *B*[2 000] (only the major Phe32*B* orientations shown).

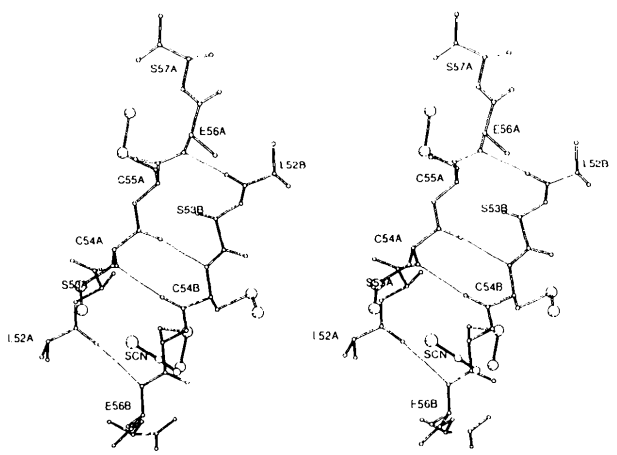

Fig. 12. Close-up view of the intermolecular β-sheet between molecules *A* and *B*. The side chains of Leu, Ser and Glu are omitted for clarity, only the disulfide bridges 43→54 and 55→60 are indicated. The twofold non-crystallographic axis runs perpendicular to the figure across the Cys54*A*/Cys54*B* pairing. The SCN^- anion is located ≅ 3 Å away from the axis.

in Table 11. This arrangement brings the two Phe32*A*/Trp29*B* and Trp29*A*/Phe32*B* residues into close mutual staggered contact. Interestingly, these two residues are functionally important as demonstrated by site-directed mutagenesis experiments (Pillet & Ménez, in preparation).

(3) *The thiocyanate.* In the monomeric form of erabutoxin-b, there is one sulfate ion in a positive pocket at the N-terminus which is made up of Arg1 and the two symmetry-related Asn5 and Lys15 residues. This pocket no longer exists in the dimeric structure and the environment of the N-terminal is essentially void of any electron density, with the exception of solvent molecules. The thiocyanate ion, the density of which was unequivocal, was clearly localized in the vicinity of the intermolecular β-sheet association (Figs. 12 and 13) and positioned in the proximity (2.9 Å) of the non-crystallographic binary axis which runs perpendicularly across the intermolecular β-sheet in the middle of the Cys54*A*/Cys54*B* dimer.

This ion is located in a polar cave (Fig. 13) delimited by the three molecules *A*[1 000], *B*[1 000] and *A*[3 001]. The sum of van der Waals radii of S and NH_3 groups (1.9 and 1.5 Å respectively; Wells, 1984), is compatible with short contacts with Ser23*B* and the positively charged symmetry-related Arg33*A*[3 001] side chain (2.7 and 3.3 Å, respectively) plus a water molecule (d[S→*W*3–2] = 3.4 Å) which bridges the *A* and *B* molecules of the dimer. These contacts are mainly directed towards the N atom. From the bond lengths and angles of the thiocyanate molecule, a negative charge was initially assumed on the S atom (d_{NC} = 1.17, d_{CS} = 1.65 Å, Batts, Coppens & Kvick, 1977), but it is noteworthy

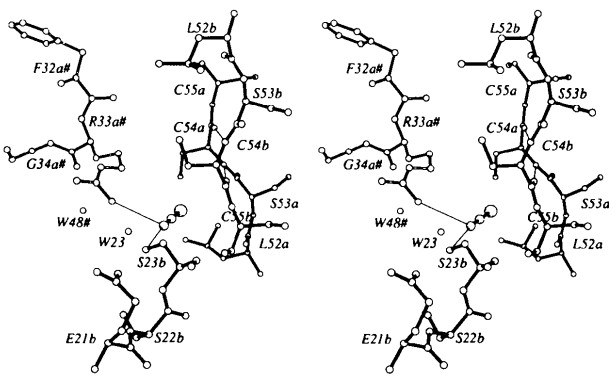

Fig. 13. The polar cave delimited by the three *A*[1 000], *A*[3 001] and *B*[1 000] molecules of the packing around the thiocyanate ion. Two molecules of water are also implicated in the hydrogen-bond network. The anti-parallel intermolecular β-sheet between *A*[1 000] (thick line) and *B*[1 000] (dashed line) is side viewed at the right. Three other loops come close to the thiocyanate, one belongs to *B*[1 000] (middle), the two others are from the symmetry-related *A*[3 001] (light tracing, left).

Table 11. *Hydrogen bonding and short contacts between molecules in the packing*

Atoms	Distances (Å)
(1) β-sheet association between *A*[1 000] and *B*[1 000]	
O Leu52*B*→N Glu56*A*	3.06
N Cys54*B*←O Cys54*A*	2.93
O Cys54*B*→N Cys54*A*	2.84
N Glu56*B*←O Leu52*A*	3.13
(2) Interleaving contacts between *A*[1 000] and *B*[2 000]	
N Ser30*A*←O Ser30*B*	3.3
O Pro48*A*→*OG* Ser30*B*	3.51
O Pro48*A*→*OG*1 Thr35*B*	3.6
O Gly49*A*→*OG* Ser30*B*	3.6
Phe/Trp interaction:	
CZ Phe32*A*↔*CE*2 Trp29*B*	3.11
(3) Thiocyanate bonding	
N SCN→*OG* Ser23*B*	2.68
N SCN→NH1 Arg33*A*	3.26
S SCN→O Cys54*B*	3.31
S SCN→*W*23	3.43

(Cotton & Wilkinson, 1972) that the electronic state of the thiocyanate ion in complexes depends on several factors, including the nature of the ligands and the character of the solvent. Though it is difficult at a resolution of 1.7 Å to discriminate between the two isoforms of thiocyanate, the bond distances at the SCN^- ion given in Table 11 support the isothiocyanate form with a charged nitrogen. The question remains as to whether more thiocyanate ions could be present in the packing. A survey of the other charged side chains pointing towards the surface indicates that the putatively bonded residues usually display high thermal factors (*e.g.* Lys and Arg residues). Under these conditions, it is difficult to ascertain whether the round-shaped residual electron density connected to them can be attributed to more, agitated or partially occupied thiocyanate ions. All of these peaks were treated as water molecules.

(4) *Other short contacts between molecules and water bridges.* The total number of localized water molecules is 97. They can be divided into two classes of molecules, those directly bonded to the polar atoms (the first shell of hydration) and those which are not connected to the protein and belong to the second hydration shell. As a result of the close packing, eight of them are cross-linking molecules between the first hydration shell of symmetry-related molecules.

In a recent analysis of the hydration scheme of lysozyme T4 (Bell, Wilson, Zhang, Faber, Nicholson & Matthews, 1991), it was shown that salt has only a moderate influence on the ordered hydrogen-bond network. A comparison between the monomeric/SO_4^{2-} and the dimeric/SCN^- erabutoxin-b networks indicates that despite the very different arrangement of the molecules in the packing, many equivalent sites of hydration are observed (41% in a range of 0.8 Å).

Concluding remarks

The analyses presented in this paper reveal that the backbone conformation of erabutoxin-b in this new crystal form is essentially identical to that of the 2EBX and 3EBX monomeric structures, with the exception of the side chains which are very dependent on the packing arrangement. This new crystal form essentially results from duplication around a twofold local axis, crossing the dimer in the middle of an intermolecular β-sheet association. A single thiocyanate ion is found to be closely related to this twofold axis, probably in the isothiocyanate electronic state, as deduced from its hydrogen-bonded network towards a serine and an arginine. Further work is in progress in order to define the exact role of thiocyanate as a crystallizing agent by using other model proteins.

We thank Dr André Ménez for kindly supplying the sample of erabutoxin-b and Mme Claudine Pascard for helpful discussions.

References

BATTS, J. W., COPPENS, P. & KVICK, Å. (1977). *Acta Cryst.* B**33**, 1534–1542.

BELL, J. A., WILSON, K. P., ZHANG, X. J., FABER, H. R., NICHOLSON, H. & MATTHEWS, B. W. (1991). *Proteins*, **10**, 10–21.

BERNSTEIN, F. C., KOETZLE, T. F., WILLIAMS, G. J. B., MEYER, E. F. JR, BRICE, M. D., RODGERS, J. R., KENNARD, O., SHIMANOUCHI, T. & TASUMI, M. (1977). *J. Mol. Biol.* **112**, 535–542.

BOURNE, P. E., SATO, A., CORFIELD, P. W. R., ROSEN, L. S., BIRKEN, S. & LOW, B. (1985). *Eur. J. Biochem.* **153**, 521–527.

BRÜNGER, A. (1990). *XPLOR Manual.* Version 1.5. Department of Biophysics, Yale Univ., Newhaven, CT 06511, USA.

BUSING, W. R. & LEVY, H. A. (1967). *Acta Cryst.* **22**, 457–464.

CASTELLANO, E. E., OLIVA, G. & NAVAZA, J. (1992). *J. Appl. Cryst.* **25**, 281–284.

*CCP*4 (1979). *A Suite of Programs for Protein Crystallography.* SERC Daresbury Laboratory, Warrington, England.

COTTON, F. A. & WILKINSON, G. (1972). In *Chemistry of the Transition Elements*, 3rd ed. New York: Interscience.

CROWTHER, R. A. (1972). *The Molecular Replacement Method*, edited by M. G. ROSSMANN, pp. 173–178. New York: Gordon & Breach.

CROWTHER, R. A. & BLOW, D. M. (1967). *Acta Cryst.* **23**, 544–548.

DRENTH, J., LOW, B., RICHARDSON, J. & WRIGHT, C. (1980). *J. Biol. Chem.* **255**, 2652–2655.

DUFTON, M. F. & HIDER, R. C. (1983). *CRC Crit. Rev. Biochem.* **14**, 113–171.

ENDO, T. & TAMIYA, N. (1987). *Pharmacol. Ther.* **34**, 403–451.

FITZGERALD, P. M. D. (1988). *J. Appl. Cryst.* **21**, 273–278.

FOX, G. C. & HOLMES, K. C. (1966). *Acta Cryst.* **20**, 886–891.

FRENCH, S. & WILSON, K. S. (1978). *Acta Cryst.* A**34**, 517–525.

HENDRICKSON, W. A. (1985). *Methods Enzymol.* **115**, 252–270.

HUBER, R. & SCHNEIDER, M. (1985). *J. Appl. Cryst.* **18**, 165–169.

JONES, T. A. (1978). *J. Appl. Cryst.* **11**, 614–617.

KENNARD, O., CRUSE, W., NACHMAN, J., PRANGÉ, T., SHAKKED, Z. & RABINOVITCH, D. (1986). *J. Mol. Dyn.* **3**, 623–647.

KONNERT, J. H. & HENDRICKSON, W. A. (1980). *Acta Cryst.* A**36**, 344–350.

LOVE, R. A. & STROUD, M. (1986). *Protein Eng.* **1**, 37–46.

LOW, B. (1979). *Handb. Exp. Pharmacol.* **52**, 213–257.

LOW, B. & CORFIELD, P. W. R. (1986). *Eur. J. Biochem.* **161**, 579–587.

LOW, B., POTTER, R., JACKSON, R. B., TAMIYA, N. & SATO, S. (1971). *J. Biol. Chem.* **246**, 4366–4368.

LOW, B., PRESTON, H. S., SATO, A., ROSEN, L. S., SEARL, J. E., RUDKO, A. D. & RICHARDSON, J. S. (1976). *Proc. Natl Acad. Sci. USA*, **73**(9), 2991–2994.

MÉNEZ, A. (1987). *Recherche*, **18**, 886–893.

MÉNEZ, R. & DUCRUIX, A. (1990). *J. Mol. Biol.* **216**, 233–234.

MÉNEZ, R. & DUCRUIX, A. (1991). In preparation.

MOSS, D. S. (1985). *Acta Cryst.* A**41**, 470–475.

NAVAZA, J. (1987). *Acta Cryst.* A**43**, 645–653.

NAVAZA, J. (1990). *Acta Cryst.* A**46**, 619–620.

OTWINOWSKI, Z. (1988). *DENZO. A Program for Automatic Evaluation of Film Densities.* Department of Biophysics, Yale Univ., Newhaven, CT 06511, USA.

RAMAKRISHNAN, C. & RAMACHANDRAN, G. M. (1965). *Biophys. J.* **5**, 909–933.

REES, B., BILWES, A., SAMAMA, J. P. & MORAS, D. (1990). *J. Mol. Biol.* **214**, 281–297.

REES, B., SAMAMA, J. P., THIERRY, J. C., GILIBERT, M., FISCHER, J., SCHWEITZ, H., LAZDUNSKI, M. & MORAS, D. (1987). *Proc. Natl Acad. Sci.* **84**, 3132–3136.

RIÈS-KAUTT, M. & DUCRUIX, A. (1989). *J. Biol. Chem.* **264**, 745–748.

RIÈS-KAUTT, M. & DUCRUIX, A. (1991). *J. Cryst. Growth*, **101**, 20–25.

SMITH, J. L., CORFIELD, P. W. R., HENDRICKSON, W. A. & LOW, B. (1988). *Acta Cryst.* A**44**, 357–368.

TAMIYA, N. & ARAI, H. (1966). *Biochem. J.* **99**, 624–630.

TICKLE, I. (1985). *Molecular Replacement*, edited by P. A. MACHIN, pp. 22–26. SERC Daresbury Laboratory, Warrington, England.

TSERNOGLOU, D. & PETSKO, G. A. (1976). *FEBS Lett.* **68**, 1–4.

WALLER, D. A. & LIDDINGTON, R. C. (1990). *Acta Cryst.* B**46**, 409–418.

WELLS, A. F. (1984). In *Structural Inorganic Chemistry.* Oxford: Clarendon Press.